Temperature Dependence of Rate Constants for $Tb^{3+}(^5D_3)$ Cross Relaxation in Symmetric Tb^{3+} Pairs in Tb-Doped $CsCdBr_3$, $CsMgBr_3$, $CsMgCl_3$

Tricia A. Lawrence, Katherine A. Murra, and P. Stanley May*

Department of Chemistry, University of South Dakota, Vermillion, South Dakota 57069

Received: September 18, 2002; In Final Form: January 24, 2003

Microscopic rate constants for $Tb(^5D_3)$ cross relaxation have been determined as a function of temperature in symmetrical $Tb^{3+}-Tb^{3+}$ pairs in $CsCdBr_3$, $CsMgBr_3$ and $CsMgCl_3$. The temperature dependence and maximum efficiency of cross relaxation is very different in the three hosts, despite the fact that the energy-level structures and luminescence spectra are quite similar. The difference in cross relaxation behavior in the three systems is due to the fact that the degree of resonance is the dominant factor in determining transfer efficiencies, easily outweighing the influences of general transition strengths and donor−acceptor separations. Only donor and acceptor transitions with significant overlap of the zero-phonon spectral lines participate in active transfer mechanisms. The temperature dependence of cross relaxation is due to the changing thermal populations of the initial crystal-field levels of resonant donor and acceptor transitions. All transitions in resonance involve a "hot" crystal-field transition, either on the donor, on the acceptor, or on both. The marked differences in the temperature dependence of cross relaxation in the three systems are attributed to slight differences in crystal-field energy-level structures, which, in turn, result in different crystal-field transitions being in resonance in the three systems. Although phonon-assisted processes are not discounted, they do not appear to have a significant impact on the temperature dependence of cross relaxation. Crystal-field analyses for Tb^{3+} in symmetric pairs in the three hosts are also reported.

1. Introduction

We are engaged in a systematic study of resonant electronic energy transfer in isolated pairs of trivalent lanthanide ions (Ln^{3+}) in a series of $CsMX_3$ halides, $CsCdBr_3$, $CsMgBr_3$, and $CsMgCl_3$, all of which adopt the hexagonal $CsNiCl_3$ structure. These compounds belong to the space group $P6_3/mmc$, in which the halide ions form infinite chains of face-sharing octahedra running parallel to the c_3 crystal axis. The divalent ions reside at the centers of the octahedra and the Cs^+ ions lie between the infinite chains. The $[MX_6]^{4-}$ octahedra are slightly elongated along the c_3 axis, so that the site symmetry of the divalent ion is D_{3d}. Trivalent lanthanides are known to enter these lattices predominately as a single type of symmetrical pair, $Ln^{3+}-(M^{2+}$ vacancy$)-Ln^{3+}$, with each pair substituting for three M^{2+} ions.[1] The lanthanides in the symmetric pair collapse slightly toward the M^{2+} vacancy, lowering their site symmetry to C_{3v}.

$CsCdBr_3$ is by far the most studied of the three lattices, owing largely to the fact that it is the most-easily synthesized and the least hygroscopic. Optical studies and/or 4f energy-level analyses of Ln^{3+} ions in $CsCdBr_3$ include singly doped Ce^{3+},[2] Pr^{3+},[3−12] Nd^{3+},[13−19] Eu^{3+},[20] Tb^{3+},[21−23] Dy^{3+},[13,24,25] Ho^{3+},[13,26−30] Er^{3+},[13,14,31−37] Tm^{3+},[6,13,38,39] and Yb^{3+} [40−45] systems and co-doped $Tb^{3+}-Gd^{3+}$,[21] $Tm^{3+}-Pr^{3+}$,[6,46] $Tm^{3+}-Ho^{3+}$,[39] $Yb^{3+}-Er^{3+}$,[47] $Pr^{3+}-Gd^{3+}$,[13] and $Ce^{3+}-Tm^{3+}$ [48] systems. The tendency for Ln^{3+} ions to form pairs in these compounds greatly facilitates energy transfer and cooperative optical processes between Ln^{3+} ions, and a number of the systems referenced above have been shown to exhibit luminescence upconversion, in which the observed emission wavelengths are shorter than the excitation wavelength.[6,8−11,16,18,19,25,26,28−37,39,40,42−44,46,47]

In contrast, only a few studies of the optical properties of Ln^{3+} ions in $CsMgCl_3$ and $CsMgBr_3$ have appeared in the literature. Ghavari and McPherson have reported visible-to-UV upconversion in $Gd^{3+}-Er^{3+}$ codoped $CsMgCl_3$, in which excited pairs of Er^{3+} ions cooperatively transfer electronic energy to Gd^{3+} ions, which, in turn, emit UV light.[49] McPherson et al. have also published an interesting comparative study of upconversion luminescence from simultaneously excited pairs of Er^{3+} ions in all three $CsMX_3$ lattices.[34] Xiao et al. have reported the temperature dependence of the microscopic rate constants for $Eu^{3+}(^5D_2)$ and $Eu^{3+}(^5D_1)$ cross-relaxation in symmetrical Eu^{3+} pairs in $CsMgCl_3$.[50]

In addition to being efficient hosts for Ln^{3+} upconversion processes, the $CsMX_3$ lattices also serve as excellent model systems for the characterization of many important energy transfer processes between lanthanide ions. Because Ln^{3+} ions have a strong tendency to enter the host lattice as a single type of $Ln^{3+}-Ln^{3+}$ pair, energy transfer between Ln^{3+} ions is reduced to a single-donor/single-acceptor environment, enabling unambiguous spectroscopic determination of microscopic transfer rates and facilitating detailed calculations of mechanistic contributions to the transfer rate without relying on problematic assumptions regarding the donor environment. The goals of this research are to use optical spectroscopic methods to accurately determine microscopic transfer rates between lanthanide ions for various donor−acceptor pairs in a series of $CsMX_3$ halides, to identify the electronic energy levels involved in the transfer processes, to calculate the expected contributions of direct multipole−multipole interactions to the transfer rate using spectroscopic data and semiempirical 4f wave functions to determine the relevant transition dipole and quadrupole strengths, and to assess the importance of indirect transfer mechanisms in which halide ions actively facilitate transfer. The results of this study will be useful not only in critically evaluating the *nature* of the physical interactions responsible for electronic energy transfer in these important upconversion materials but

* To whom correspondence should be addressed. E-mail: smay@usd.edu.

10.1021/jp0270248 CCC: $25.00
Published on Web 04/08/2003

also in determining the most important parameters influencing absolute transfer efficiency.

In this paper, we present a comparative study of cross-relaxation of Tb^{3+} in the $^5D_3$ state by Tb^{3+} in the $^7F_6$ ground state in symmetric $Tb^{3+}-Tb^{3+}$ pairs in $CsCdBr_3$, $CsMgBr_3$, and $CsMgCl_3$. We have determined the microscopic rate constants for cross relaxation as a function of temperature from 8−298 K. We find that the relative temperature-dependent behavior can be very well described in terms of resonance of zero-phonon donor and acceptor transitions and the Boltzmann populations of the initial crystal-field levels of the donor and/or acceptor transitions. The marked differences in the temperature dependence of cross relaxation in the three systems are attributed to slight differences in crystal-field energy-level structures, which, in turn, result in different crystal-field transitions being in resonance in the three systems. We note that the ability to *compare* the temperature dependence of the rate constants for the three compounds was extremely useful in removing the ambiguity of interpretation which would have been associated with analyzing the temperature dependence in any single lattice.

2. Experimental Section

2.1. Synthesis and Crystal Growth. The preparation of the 0.2% Tb: $CsCdBr_3$ and 1%Gd: 0.1%Tb: $CsCdBr_3$ crystals used in this study is described in ref 21.

$CsMgBr_3$ was prepared by reacting $CsCdBr_3$ with a slight molar excess of Mg metal by heating the mixture under vacuum in a Vycor tube. The cadmium metal produced in the reaction sublimes onto the inner portion of the Vycor tube above the reaction mixture. A single crystal of the resulting $CsMgBr_3$ was grown using the Bridgman method with a maximum furnace temperature of 650 °C. Portions of the crystal with the highest optical quality were combined with the appropriate anhydrous lanthanide bromides and returned to the Bridgman furnace. The $CsMgBr_3$ crystals used in this study are nominally 0.48% Tb: $CsMgBr_3$ and 1% Gd:0.1% Tb:$CsMgBr_3$.

The anhydrous lanthanide bromides used to dope $CsCdBr_3$ and $CsMgBr_3$ were prepared from the lanthanide oxides and ammonium bromide via the so-called "dry route".[51]

$CsMgCl_3$ was prepared by fusing equimolar amounts of anhydrous CsCl and $MgCl_2$ under vacuum. The resulting samples were then sealed under vacuum in 9 mm Vycor ampules, and single crystals were grown from melt via the Bridgman method with a maximum furnace temperature of 650 °C. Portions of the crystal boules with the highest optical quality were then selected, combined with the appropriate anhydrous lanthanide chloride(s), sealed under vacuum, and returned to the Bridgman furnace. In this study, the nominal concentration of the Tb-doped $CsMgCl_3$ crystal was 0.2% Tb, and the concentrations of the Tb−Gd codoped $CsMgCl_3$ crystal was 0.2% Gd and 0.1% Tb.

2.2. Spectroscopic Measurements. High-resolution luminescence/excitation spectra and time-dependent luminescence data were acquired using a PC-controlled system consisting of nitrogen laser/dye laser excitation (Laser Photonics models UV-12 and DL-14, respectively), a 0.46M flat-field monochromator (Jobin-Yvon HR460), and a time-resolved photon-counting detection system consisting of a fast, red-sensitive, side-window photomultiplier (Hamamatsu R2949), and a multichannel scaler (Stanford Research SR430). For temperature control, samples were attached to a copper mount in the sample compartment of a closed-cycle cryostat (CRYOMECH Model ST15) using copper grease and indium foil. To avoid nonlinear processes, laser excitation powers used in these experiments were typically less than 100 μJ/pulse; also, the excitation beam was left unfocused, resulting in a 2−3 mm beam diameter at the sample. We noted no power dependence in the luminescence spectra or in the shapes of the luminescence decay curves over the range of excitation powers used.

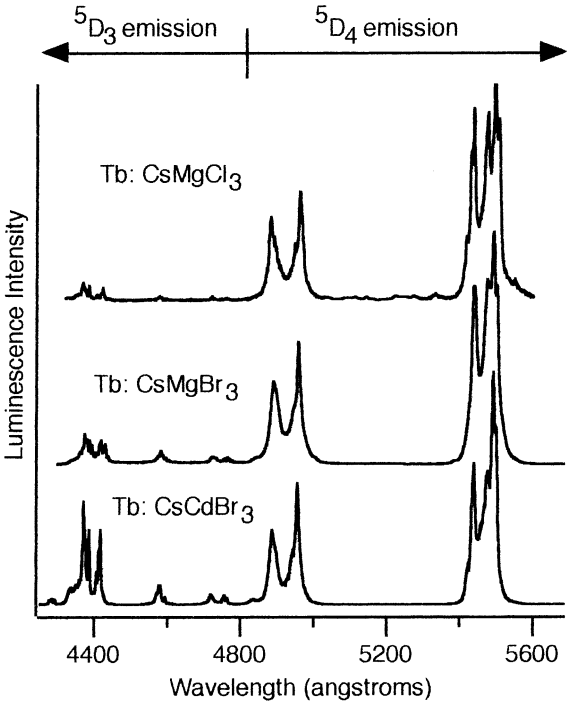

Figure 1. Comparison of a portion of the room-temperature, unpolarized Tb^{3+} luminescence spectra for Tb-doped $CsCdBr_3$, $CsMgBr_3$, and $CsMgCl_3$ obtained using excitation at 3609, 3660, and 3796 Å, respectively. Spectral resolution is 3 Å. Spectra are corrected for monochromator and detector response such that the intensities are proportional to photons counts/dλ.

3. Results and Discussion

3.1. Luminescence and Excitation Spectra. A comparison of a portion of the room-temperature Tb luminescence spectra for Tb-doped $CsCdBr_3$,$CsMgBr_3$, and $CsMgCl_3$ obtained using $^5D_3$ excitation is shown in Figure 1. Emission from both the $^5D_3$ and $^5D_4$ levels is observed, but the former is significantly quenched by the Tb−Tb cross-relaxation processes shown in Figure 2. We note that the two possible cross-relaxation pathways, labeled k_{cr1} and k_{cr2}, are spectroscopically indistinguishable, since the net result of either event is one Tb^{3+} in the $^5D_4$ state and one Tb^{3+} in the $^7F_0$ state. For the remainder of the paper, we will concentrate on the total cross-relaxation rate constant, k_{cr}, where $k_{cr} = k_{cr1} + k_{cr2}$. The relative ratios of $^5D_3$ to $^5D_4$ emission indicate that the efficiency of room-temperature cross relaxation in the three lattices goes as $CsMgCl_3$ > $CsMgBr_3$ > $CsCdBr_3$. We note that care must be exercised in evaluating relative cross-relaxation efficiencies solely on the basis of luminescence spectra, because any single ions which may be present would contribute disproportionately to $^5D_3$ emission intensity.[21] As discussed in section 3.3, however, luminescence lifetime data support the relative efficiencies given above.

Figure 3 shows a comparison of a portion of the low-temperature (8−10 K) Tb^{3+} luminescence spectra in the three lattices. An increase in the $^5D_3$ to $^5D_4$ emission ratio relative to room temperature is observed for all three compounds, indicating a decrease in cross-relaxation efficiency. Also of particular interest is the very high degree of similarity in the spectra in

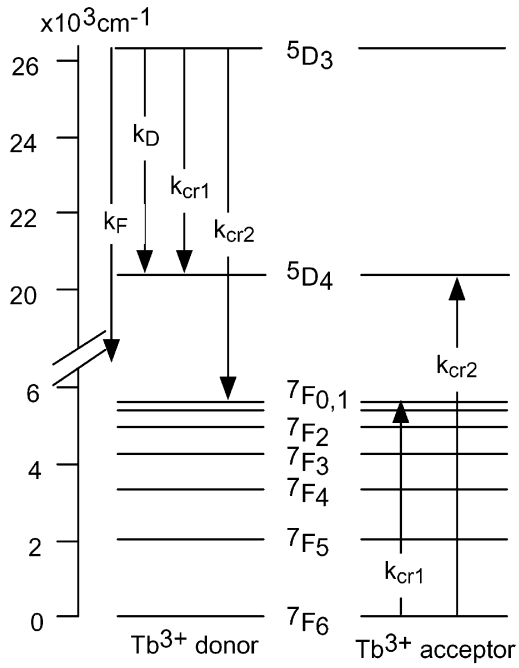

Figure 2. Schematic representation of the relaxation pathways out of the $^5D_3$ state of Tb^{3+} in symmetric Tb pairs. k_D and k_F are the rate constants for the single-ion Tb($^5D_3$) → Tb($^5D_4$) and Tb($^5D_3$) → Tb(^7F_J) relaxation processes, respectively. k_{cr1} and k_{cr2} are the rate constants for the two possible cross-relaxation pathways. The immediate result of both pathways is one Tb^{3+} ion in the $^5D_4$ state and one Tb^{3+} ion in the $^7F_0$ state.

terms of the positions and relative intensities of the crystal-field transitions within a multiplet-to-multiplet transition region. The crystal-field environment of Tb^{3+} in symmetric pairs is clearly quite similar in all three compounds.

The similarity of the crystal-field environment in the three lattices is again seen when comparing the low-temperature excitation spectra of the $^7F_6$ → $^5D_3$ and $^7F_6$ → $^5G_6$, $^5L_{10}$ regions shown in Figure 4. These spectra show that the $^5D_3$ multiplet is quite close in energy (~100 cm^{-1}) to the adjacent higher-energy multiplets, $^5G_6$ and $^5L_{10}$. The close proximity of these levels to $^5D_3$ significantly affects the temperature dependence of the thermal population of the $^5D_3$ crystal-field levels following direct $^5D_3$ excitation and, consequently, influences the temperature dependence of the cross-relaxation rate constants. Also, it seems probable that, in Tb:$CsMgCl_3$, important resonant donor transitions originate from these upper-lying levels at higher temperatures (See section 3.4).

3.2. Energy Levels and Crystal-Field Analysis. The location for the majority of the $^5D_3$, $^5D_4$, and ^7F_J ($J = 0-6$) crystal-field levels for symmetric Tb^{3+} pairs in $CsCdBr_3$, $CsMgBr_3$, and $CsMgCl_3$ are given in Table 1. Assignments were made on the basis of the temperature dependence of emission and excitation spectra. For a few multiplets, the location of all crystal-field levels could not be determined. No experimental determination of the symmetry of the crystal-field levels was attempted. The irreducible representation labels in Table 1 are those of the wave functions resulting from a crystal-field energy-level analysis (described below). For the $^7F_3$ multiplet, the relative position of the unlocated level within the multiplet could not be determined, so that it was not possible to correlate experimental and calculated levels.

Comparing the energy-level structures of Tb^{3+} pairs in the two bromide lattices, one sees that the crystal-field *splittings* in $CsMgBr_3$ and $CsCdBr_3$ are nearly identical. Overall, the *pattern* of crystal-field splittings in the $CsMgCl_3$ lattice mirror those seen in $CsCdBr_3$ and $CsMgBr_3$, but the *magnitude* of the splittings is slightly larger. The SLJ multiplets of $CsMgBr_3$ are shifted to slightly lower energies relative to $CsCdBr_3$. The lower multiplet energies in $CsMgBr_3$ is consistent with the smaller Tb^{3+}−Br separation compared to $CsCdBr_3$, leading to greater cation−anion interaction, which, in turn, leads to an expansion of the 4f wave functions and a decrease in Coulombic repulsion between the 4f electrons. The higher multiplet energies of $CsMgCl_3$ relative to both bromide lattices is similarly explained in terms of chloride ligands being generally less effective in expanding the 4f wave functions relative to the bromides. The correlation of SLJ energy shifts to lower energies with decreasing lanthanide−halide bond lengths and with decreasing "ionicity" of the halide ligand has been convincingly demonstrated in the rare earth trihalides.[52]

Crystal-field energy-level analyses of symmetric Tb^{3+} pairs in $CsCdBr_3$ and $CsMgCl_3$ were performed for C_{3v} site symmetry using programs provided to us by M. F. Reid at the University of Canterbury, Christchurch, New Zealand. An intermediate-

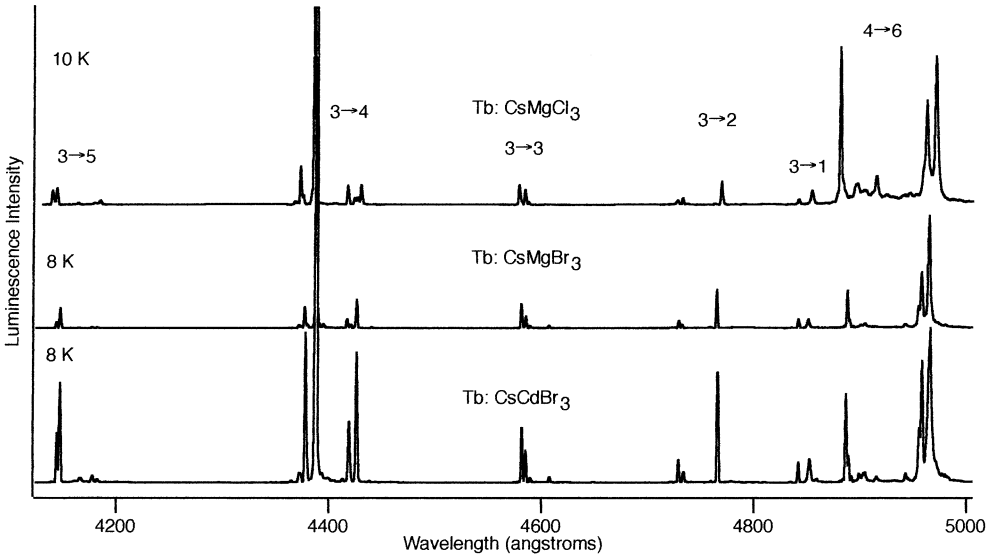

Figure 3. Comparison of a portion of the low-temperature (8−10 K) unpolarized Tb^{3+} luminescence spectra in $CsMgCl_3$ (top), $CsMgBr_3$ (middle), and $CsCdBr_3$ (bottom), exciting at 3802, 3809, and 3808 Å, respectively. Spectral resolution is 2 Å. Spectra are corrected for monochromator and detector response such that the intensities are proportional to photons counts/dλ.

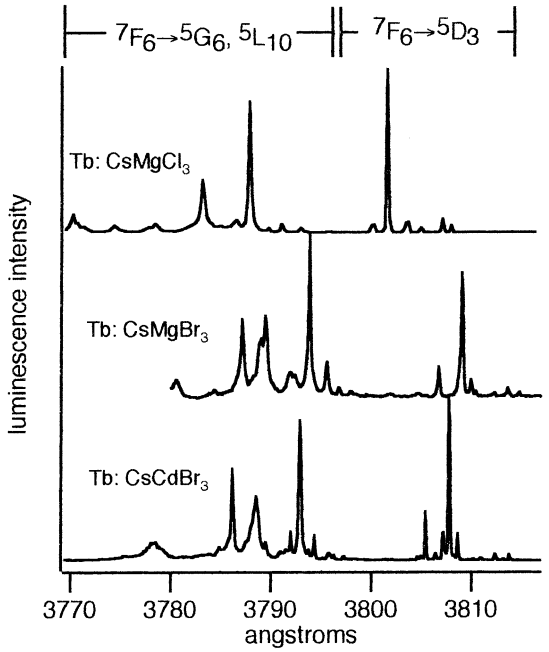

Figure 4. Low-temperature (~10 K) excitation spectra of the Tb^{3+} $^7F_6 \rightarrow {}^5D_3$ and $^7F_6 \rightarrow {}^5G_6, {}^5L_{10}$ regions in $CsMgCl_3$ (top), $CsMgBr_3$ (middle), and $CsCdBr_3$ (bottom), monitoring $^5D_3 \rightarrow {}^7F_4$ emission at ~4380 Å. These spectra show that the $^5D_3$ multiplet is quite close in energy (~100 cm^{-1}) to the adjacent higher-energy multiplets, $^5G_6$ and $^5L_{10}$. The relationship between the laser polarization and the *c*-axis was not determined.

coupling basis set generated within the $4f^8$ electron configuration was used, with a cutoff at ~38 000 cm^{-1}. The Hamiltonian, **H**, is commonly divided into free-ion, $\mathbf{H}_f$, and crystal-field, $\mathbf{H}_{cf}$, components as follows

$$\mathbf{H} = \mathbf{H}_f + \mathbf{H}_{cf} \quad (1)$$

The free-ion Hamiltonian is explicitly defined in ref 14 (in which it is referred to as $\mathbf{H}_a$). For the present study, free-ion parameters were assigned to the values reported for Tb^{3+} in LaF_3 by Carnall et al.[53] and were not varied in the calculations.

The general form of the crystal-field Hamiltonian may be written as

$$\mathbf{H}_{cf} = \sum_{k,q} B_q^k \mathbf{C}_q^k \quad (2)$$

where the $\mathbf{C}_q^k$ are intraconfigurational spherical tensor operators of rank *k* and order *q*, and the B_q^k are one-electron crystal-field interaction parameters. For C_{3v} site symmetry, the crystal-field Hamiltonian contains six crystal-field parameters, and may be written as[5b]

$$\mathbf{H}_{cf} = B_0^2\mathbf{C}_0^2 + B_0^4\mathbf{C}_0^4 + B_3^4(\mathbf{C}_3^4 - \mathbf{C}_{-3}^4) + B_0^6\mathbf{C}_0^6 + B_3^6(\mathbf{C}_3^6 - \mathbf{C}_{-3}^6) + B_3^6(\mathbf{C}_6^6 + \mathbf{C}_{-6}^6) \quad (3)$$

In our analysis, the six crystal-field parameters were optimized to give the best agreement between observed and calculated crystal-field *splittings*. Obtaining acceptable fits to "absolute" energy-level positions was not possible. This was due at least partially to the fact that our data set included crystal-field levels from only two different SL states, which severely restricted our ability to optimize free-ion electrostatic parameters. Obtaining reliable free-ion electrostatic parameters for Tb^{3+} systems is a common problem,[53] because only a small fraction of the $4f^6$ configuration lies below 50 000 cm^{-1}. A separate fit for Tb^{3+} in $CsMgBr_3$ was not performed, because, as previously stated,

TABLE 1: Crystal-Field Energy Levels (in cm^{-1}) of the ^7F_J ($J = 6-0$), $^5D_4$, and $^5D_3$ Multiplets of Tb^{3+} in Symmetric Pairs in $CsMgBr_3$, $CsCdBr_3$, and $CsMgCl_3$[a]

multiplet	calculated symmetry[b]	$CsMgBr_3$ (cm^{-1})	$CsCdBr_3$ (cm^{-1})	$CsMgCl_3$ (cm^{-1})
$^7F_6$	A_1	0	0	0
	E	21	21	23
	E	86	86	70
	A_2	102	102	78
	A_1	120	120	146
	A_2	257	252	296
	A_1	296	296	334
	E	302	306	349
	E	316	325	372
$^7F_5$	A_2	2079	2089	2092
	E	2099	2104	2118
	E	2204	2214	2233
	A_1	2215	2233	2255
	E	2275	2282	
	A_2	2300	2306	
	E		2317	2354
$^7F_4$	A_2	3327	3337	3342
	A_1	3365	3377	3380
	E	3377	3385	3396
	E	3420	3427	3447
	A_1	3569	3589	3610
	E	3616	3625	3675
$^7F_3$[c]		4382	4393	4406
		4401	4410	4434
		4419	4430	4448
		4504	4515	4546
$^7F_2$	E	5064	5073	5095
	A_1	5078	5094	5119
	E	5223	5237	5279
$^7F_1$	E	5557	5567	5592
	A_2	5597	5611	5648
$^7F_0$	A_1	5787	5803	5834
$^5D_4$	A_1	20455	20467	20479
	A_2	20468	20478	20492
	E	20473	20486	20506
	E	20479	20491	20518
	A_1		20519	20540
	E		20540	20543
$^5D_3$	A_2	26207	26216	26238
	E	26238	26247	26267
	A_1	26247	26258	26282
	E,A_2	26264	26273	26291

[a] Energies are corrected to vacuum. [b] Irreducible representations of wave functions obtained from crystal-field analysis. No experimental determination of the symmetries of the crystal-field levels was performed. [c] Calculated symmetries and experimental levels could not be correlated, since relative position of the missing level could not be determined.

TABLE 2: Crystal-Field Parameters[a] for Tb^{3+} in $CsCdBr_3$, $CsMgBr_3$, and $CsMgCl_3$

	$CsCdBr_3/CsMgBr_3$	$CsMgCl_3$
B^2_0	-193 ± 20	-218 ± 30
B^4_0	-867 ± 41	-983 ± 57
B^4_3	1030 ± 25	1215 ± 36
B^6_0	52 ± 46	-14 ± 69
B^6_3	193 ± 32	224 ± 49
B^6_6	327 ± 40	340 ± 58
no. of levels in fit	33	32
σ[b]	8 cm^{-1}	12 cm^{-1}

[a] Units are in cm^{-1}. Crystal-field parameters are reported for unit tensor normalization. [b] $\sigma = [\sum_i (E_i^{obs} - E_i^{calc})^2/(N-p)]^{1/2}$, where E_i^{obs} and E_i^{calc} are the observed and calculated energies of the *i*th crystal-field level, *N* is the number of levels used in the fit, and *p* is the number of parameters freely varied in the fit.

TABLE 3: Comparison of Crystal-Field Parameters[a] for Ln^{3+} Ions in Symmetrical Pairs in $CsCdBr_3$

	Pr^{3+}			Nd^{3+}		Eu^{3+}	Tb^{3+}	Ho^{3+}	Er^{3+}	Tm^{3+}
	ref 5	ref 7	ref 3 (fit b)	ref 17 (fit b)	ref 14	ref 20	present study	ref 27	ref 14	ref 38
B^2_0	-158 ± 30	-115	-140	-302 ± 57	-204 ± 33	-193	-193 ± 20	-151	-93 ± 36	-163
B^4_0	-1192 ± 62	-1147	-1125	-978 ± 88	-887 ± 62	-1175	-867 ± 41	-754	-601 ± 53	-656
B^4_3	1367 ± 34	1360	1417	1210 ± 58	1202 ± 42	1411	1030 ± 25	960	1104 ± 34	798
B^6_0	362 ± 73	365	242	400 ± 49	142 ± 47	302	52 ± 46	204	68 ± 31	180
B^6_3	271 ± 45	267	218	255 ± 41	207 ± 37	320	193 ± 32	169	139 ± 27	119
B^6_6	39 ± 53	15	106	-56 ± 79	400 ± 40	362	327 ± 40	158	72 ± 39	112
cf levels	40	40		48	76	16	33		65	
s	11.1	22.4		15	25.8	8.5	8		18.8	

[a] Units are in cm^{-1}. Crystal−field parameters are reported for spherical−tensor operator normalization.

the crystal-field splittings are nearly identical to the $CsCdBr_3$ system. For both fits, the initial values of the crystal-field parameters were set to those reported by Quagliano et al. for Nd^{3+} in $CsCdBr_3$.[14] The optimized crystal-field parameters for Tb^{3+} in $CsCdBr_3$, $CsMgBr_3$ and $CsMgCl_3$ are given in Table 2. Both parameter sets are quite similar. Note, however, that the larger crystal-field splittings observed for Tb^{3+} in $CsMgCl_3$ are reflected in the generally larger crystal-field parameters for this lattice.

Table 3 is a comparison of a number of crystal-field parameter sets reported for various Ln^{3+} ions in symmetrical-pair sites in $CsCdBr_3$. The uncertainties in the crystal-field parameters reported for this study are reasonable compared to those reported for other Ln^{3+} ions in $CsCdBr_3$. Except for B^6_0 and B^6_6, the crystal-field parameters values are relatively stable across the series. It is open to question as to whether the instability of the B^6_0 and B^6_6 parameters reflects real differences in crystal-field potential or is largely an artifact resulting from differences in fitting procedures, because, according to our fits, the B^6_6 parameter is strongly correlated with both B^6_0 and B^6_3. Note, for example, that the two parameter sets given in Table 3 for the same lanthanide ion, Nd^{3+}, are quite similar except for B^6_0 and B^6_6. Likewise, the ref 3 fit for Pr^{3+} is similar to those from refs 5 and 7, except for the B^6_0 and B^6_6 values. We suggest that it should be possible to obtain adequate sets of crystal-field parameters for which *all* parameters vary smoothly with across the series.

It is worth noting that the instability in B^6_0 and B^6_6 may be due in part to the exclusion of the so-called "correlated crystal-field effect" (CCF) in the fits in Table 3. The CCF takes into account two-electron crystal-field interactions by including additional parameters in the crystal-field Hamiltonian. The CCF predicts that the effective crystal potential should be a function of the spin state of the lanthanide ion. If, therefore, the CCF is not included, crystal-field parameter values may depend on the relative representation of the various spin states in the experimental energy-level data set used in the fit. For Nd^{3+} in $CsCdBr_3$, the B^6_0 and B^6_6 values are those most effected by inclusion of CCF.[14] The differences in the two fits for Nd^{3+} in Table 3 may, therefore, be at least partly attributable to differences in the data sets used.

Finally, we point out that caution must be exercised when comparing sets of crystal-field parameters from different sources; some "instabilities" observed in the literature have resulted from comparisons of parameter sets based on different normalizations of the crystal-field potential.

3.3. Luminescence Decay Measurements: Determination of Cross Relaxation Rate Constants. Figure 5 shows a comparison of the $Tb(^5D_3)$ luminescence decay curves obtained from 0.2% Tb:$CsCdBr_3$ and 1% Gd:0.1% Tb:$CsCdBr_3$ at room temperature, following direct excitation into $^5D_3$. The longer-lived emission in the Tb−Gd doped sample is consistent with emission mainly from Tb−Gd pairs, in which no cross-relaxation processes are active. $Tb(^5D_3)$ emission from Tb−Gd-doped samples is dominated by Tb−Gd pairs, because of the high concentration ratio of Gd^{3+}-to-Tb^{3+}. The decay curves shown in Figure 5 are representative of those obtained in all three lattices, namely, that Tb-doped samples are dominated by shorter-lived emission from Tb−Tb pairs and Tb−Gd-doped samples are dominated by longer-lived emission from Tb−Gd pairs.

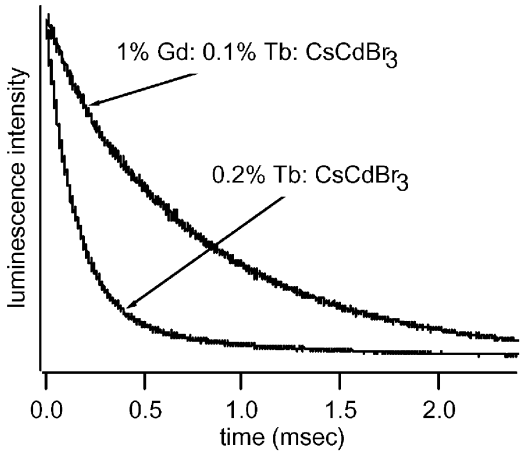

Figure 5. Comparison of $Tb(^5D_3)$ luminescence decay curves (monitoring at 4373 Å) obtained from 0.2% Tb:$CsCdBr_3$ and 1% Gd:0.1% Tb:$CsCdBr_3$ at room temperature, following direct excitation at 3796 Å into $^5D_3$.

The $Tb(^5D_3)$ decays curves for Tb−Gd-doped samples were analyzed using

$$I(t)_{\text{Tb-Gd doped}} = I(0)e^{-k_{\text{tot}}(\text{Tb-Tb pairs})t} + I'(0)e^{-k_{\text{tot}}(\text{Tb-Gd pairs})t} \quad (4)$$

It was necessary to include contributions from Tb−Tb pairs in the fits, because, although small, they were still detectable. The values obtained for k_{tot}(Tb−Tb pairs) from measurements on Tb−Gd-doped samples were strongly temperature dependent and in good agreement with those obtained from the Tb-doped samples. The values of k_{tot}(Tb−Gd pairs) were largely insensitive to temperature.

For some of our Tb-doped samples, we observed a weak, long-lived contribution to the $^5D_3$ decay curves, which never constituted more than 10% of the total initial intensity, with a rate constant quite similar to that obtained for Tb−Gd pairs. The most probable origin of this emission is from Tb^{3+} in nonpair sites, as suggested by Berdowski et al. in their study of 0.2% Tb: $CsCdBr_3$.[23] We have previously confirmed that the weak, longer-lived emission in 0.2% Tb:$CsCdBr_3$ is indeed due to Tb^{3+} ions,[21] and the fact that this emission is not quenched by cross-relaxation is consistent with emission from Tb^{3+} ions

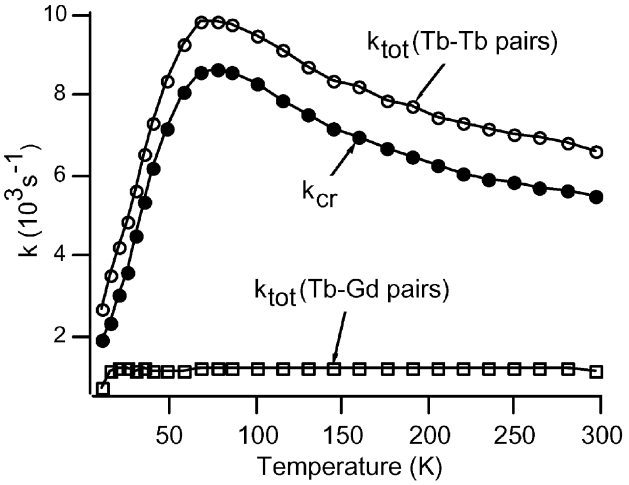

Figure 6. Temperature dependence of the $Tb(^5D_3)$ total relaxation rate constants, k_{tot}, in Tb−Tb pairs and Tb−Gd pairs, and of the total Tb-$(^5D_3)$ cross relaxation rate constant in Tb−Tb pairs, k_{cr}. Values of k_{cr} were determined from the difference in the values of k_{tot} for Tb−Tb and Tb−Gd pairs, according to eq 7.

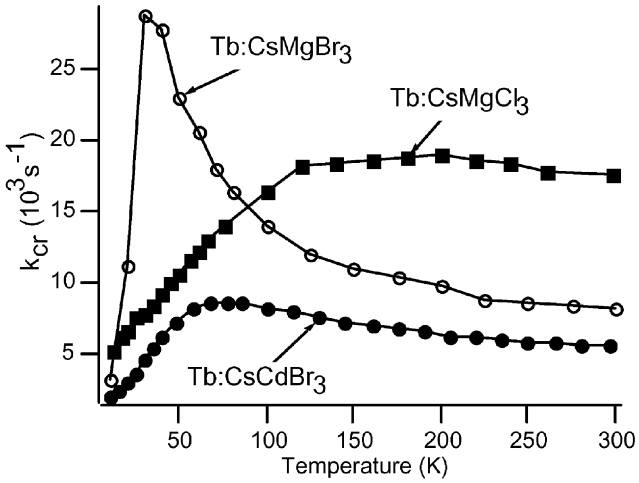

Figure 7. Comparison of the temperature dependence of the $Tb(^5D_3)$ cross-relaxation rate constant, k_{cr}, in symmetric Tb pairs for the three $CsMX_3$ lattices.

in isolated, nonpair sites. A number of other studies also report the detection of lanthanide ions in nonpair sites in these lattices.[1,2,8,9,10,12,17−20,29,38] $Tb(^5D_3)$ decay curves for Tb-doped samples were, therefore, analyzed using either

$$I(t)_{\mathrm{Tb-doped}} = I(0)\mathrm{e}^{-k_{\mathrm{tot}}(\mathrm{Tb-Tb\ pairs})} \quad (5)$$

or

$$I(t)_{\mathrm{Tb-doped}} = I(0)\mathrm{e}^{-k_{\mathrm{tot}}(\mathrm{Tb-Tb\ pairs})t} + I'(0)\mathrm{e}^{-k_{\mathrm{tot}}(\mathrm{Tb\ single\ ions})t} \quad (6)$$

The microscopic rate constants for total $Tb(^5D_3)$ cross relaxation, k_{cr}, were determined by comparing the values of k_{tot}(Tb−Tb pairs) and k_{tot}(Tb−Gd pairs) obtained from Tb-doped and Tb−Gd-doped crystals, respectively. Referring to Figure 2, k_{tot}(Tb−Tb pairs) $= k_F + k_D + k_{cr1} + k_{cr2}$ and k_{tot}(Tb−Gd pairs) $= k_F + k_D$, where k_D and k_F are the rate constants for the intrinsic $Tb(^5D_3) \rightarrow Tb(^5D_4)$ and $Tb(^5D_3) \rightarrow Tb(^7F_J)$ relaxation processes, respectively. Making the reasonable assumption that k_F and k_D are identical for Tb−Tb and Tb−Gd pairs

$$k_{cr} = k_{cr1} + k_{cr2} = k_{tot}(\mathrm{Tb-Tb\ pairs}) - k_{tot}(\mathrm{Tb-Gd\ pairs}) \quad (7)$$

To illustrate the relationship given by eq 7, Figure 6 shows a plot of k_{tot}(Tb−Tb pairs), k_{tot}(Tb−Gd pairs), and k_{cr} as a function of temperature for the $CsCdBr_3$ lattice. The temperature dependence of k_{tot}(Tb−Tb pairs) is clearly due to the temperature dependence of k_{cr}.

Figure 7 shows a comparison of the temperature dependence of the $Tb(^5D_3)$ cross-relaxation rate constant, k_{cr}, for the three lattices. The pronounced differences in the temperature dependence of cross relaxation in these compounds is remarkable, given the similarity of the Tb−Tb pair sites that is suggested by the spectral data. Also of interest is the fact that, in the $CsCdBr_3$ and $CsMgBr_3$ lattices, cross-relaxation efficiency initially increases, but then decreases with increasing temperature. The effect is particularly dramatic in $CsMgBr_3$, in which maximum cross-relaxation efficiency is reached at ∼35 K, and is followed by a precipitous drop upon further temperature increase. This behavior cannot be explained in terms of phonon occupancy and must be due to changes in the thermal populations of the electronic crystal-field levels of the $Tb(^5D_3)$ donor and the $Tb(^7F_6)$ acceptor. Our analysis of the temperature dependence of the resonance between donor and acceptor transitions presented in section 3.4 strongly supports this conclusion.

TABLE 4: Intrinsic Room Temperature Decay Constants for $^5D_3$ and $^5D_4$ Emission of Tb^{3+} in Symmetric Pairs in $CsCdBr_3$, $CsMgBr_3$, and $CsMgCl_3$

	$^5D_3$ (s^{-1})[a]	$^5D_4$ (s^{-1})
$CsCdBr_3$	1217	885
$CsMgBr_3$	1249	- - - - -
$CsMgCl_3$	775	554

[a] Determined from Tb^{3+} emission in $Tb^{3+}-Gd^{3+}$ pairs.

The lack of temperature dependence for $Tb(^5D_3)$ decay constants in Tb−Gd pairs indicates that relaxation in these pairs is largely radiative. Also, there are no cross-relaxation mechanisms quenching $Tb(^5D_4)$ emission, so that its decay characteristics are the same in Tb−Tb and Tb−Gd pairs and are also predominately radiative. The room-temperature decay constants for $Tb(^5D_3)$ emission in Tb−Gd pairs and for $Tb(^5D_4)$ emission is given for the three $CsMX_3$ lattices in Table 4. Further indication that the rate constants in Table 4 are radiative is the fact that the ratio of the $^5D_3$ to $^5D_4$ rate constants is very similar in $CsMgCl_3$ and $CsCdBr_3$. This would be unlikely if either $^5D_3$ or $^5D_4$ had significant intrinsic nonradiative deactivation.

The rate constants in Table 4 are, therefore, useful measures of the relative transition strengths in the $CsMX_3$ systems. The dipole strengths for the two bromide lattices are very similar, but both are ∼1.5 times greater than those for the chloride lattice. This may be due, at least partially, to the greater polarizability of the bromide relative to the chloride ligands, to the increased covalency of the lanthanide-bromide bond relative to the lanthanide-chloride bond, or to both. Reisfeld and Jorgensen have linked increasing covalency of the lanthanide−ligand bond with an increase in the Judd-Ofelt Ω_λ ($\lambda = 2$) electric-dipole intensity parameter.[54,55] In addition, the dynamic coupling mechanism predicts an increase in Ω_2 with increasing ligand polarizability.[55] Both mechanisms would follow the sequence of electric-dipole intensity enhancement of $I^- > Br^- > Cl^-$.

Gruen et al. have studied the vapor phase $4f \rightarrow 4f$ spectra of the tri-bromides and tri-iodides of Pr, Nd, Er, and Tm and observed greater electric-dipole intensity in the iodides relative to the bromides.[55,56] The effect, however, was manifested mainly

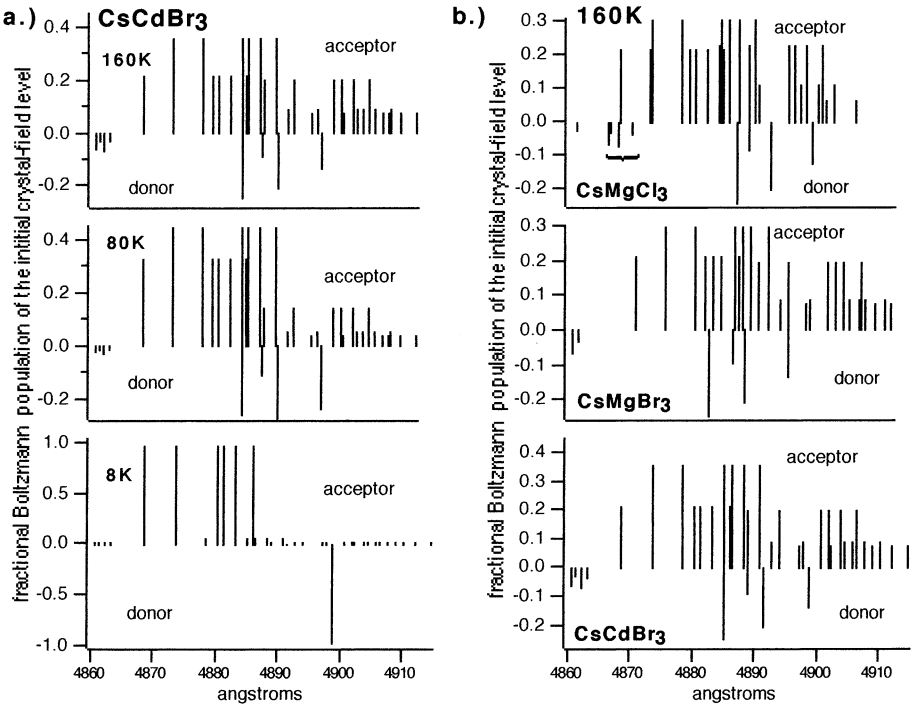

Figure 8. (a) Calculated line spectra for $^5D_3 \rightarrow {}^7F_0$ emission and $^7F_6 \rightarrow {}^5D_4$ absorption in $CsCdBr_3$ at 8, 80, and 160K. (b) Comparison of the 160 K calculated line spectra for $^5D_3 \rightarrow {}^7F_0$ emission and $^7F_6 \rightarrow {}^5D_4$ absorption in $CsMgCl_3$, $CsMgBr_3$, and $CsCdBr_3$. "Negative" lines represent donor transitions, and "positive" lines represent acceptor transitions. Each line represents a single crystal-field transition, with line height being proportional to the thermal population of the initial crystal-field level. Transition energies were determined from the energy levels in Table 1. The curly bracket in $CsMgCl_3$ donor spectrum in Figure 8b indicates where $^5G_6$,$^5L_{10} \rightarrow {}^7F_0$ emission is in resonance with $^7F_6 \rightarrow {}^5D_4$ absorption.

in the hypersensitive transitions, which were the focus of their study. Because hypersensitivity has not been observed for Tb,[55] it is unclear as to whether the increased electric-dipole intensity we observe in our bromide lattices can be accounted for solely in terms of mechanisms that primarily affect the Ω_2 parameter. This parameter is usually ill-determined in intensity-parameter fits that lack hypersensitive transitions in the experimental data sets, reflecting its generally weak effect on nonhypersensitive transitions.[55] It may be necessary to consider the relative positions of charge transfer and/or $4f^{N-1}5d$ states in the bromides and chlorides, because these would effect the mixed-parity character of the 4f wave functions. The importance of the positions of these states (relative to the $4f^N$ configuration) to electric-dipole intensities of 4f → 4f transitions has been discussed in some detail by Blasse.[57] The position of the $4f^{N-1}5d$ states is not particularly sensitive to ligand identity, but, certainly, the ligand-to-metal charge transfer state should be lower in $CsCdBr_3$ and $CsMgBr_3$ relative to $CsMgCl_3$.[55] In any case, intensity parameters for these systems would be useful in evaluating the mechanisms responsible for our observed intensity differences.

3.4. Analysis of Cross-Relaxation Behavior. Referring to the Tb^{3+} energy-level diagram in Figure 2, the two resonant spectral regions for $Tb(^5D_3)$-donor emission and $Tb(F_6)$-acceptor absorbance are $^5D_3 \rightarrow {}^7F_0/{}^7F_6 \rightarrow {}^5D_4$, centered at ~20 450 cm^{-1} (4890 Å), and $^5D_3 \rightarrow {}^5D_4/{}^7F_6 \rightarrow {}^7F_0$, centered at ~5750 cm^{-1} (17 390 Å). The actual donor-emission and acceptor-absorption spectra for these regions cannot be compared directly, because we have spectral data only for $^7F_6 \rightarrow {}^5D_4$. However, because the location of the crystal-field levels of all the relevant multiplets is known (with the exception of the two highest levels of the $^5D_4$ multiplet of $CsMgBr_3$), the relative degree of resonance between the various zero-phonon crystal-field transitions of the donor and acceptor can be evaluated.

Figure 8a shows the calculated line spectra for $^5D_3 \rightarrow {}^7F_0$ emission and $^7F_6 \rightarrow {}^5D_4$ absorption in $CsCdBr_3$ at temperatures of 8, 80, and 160 K. (The corresponding spectra for $CsMgCl_3$ and $CsMgBr_3$ are qualitatively similar.) "Negative" lines represent donor emission transitions, and "positive" lines represent acceptor absorption transitions. Each line represents a single crystal-field transition, with line height being proportional to the thermal population of the initial crystal-field level. Transition energies were determined from the energy levels in Table 1. The energies of the upper two $^5D_4$ levels of $CsMgBr_3$ were estimated by assuming that the crystal-field splittings within this multiplet are the same as that in $CsCdBr_3$. As discussed in section 3.2, this should be a quite good estimation.

To accurately calculate the thermal population of the $^5D_3$ levels, it was necessary to include crystal-field levels from the adjacent, higher-energy $^5G_6$ and $^5L_{10}$ multiplets (see section 3.1). The position of the lowest of these levels was estimated from $^7F_6 \rightarrow {}^5D_3$ excitation spectra (see Figure 4). The positions of the remaining levels were estimated from the crystal-field splittings calculated in our crystal-field analysis.

The calculated 8K line spectra show negligible resonance between the $^5D_3 \rightarrow {}^7F_0$ and $^7F_6 \rightarrow {}^5D_4$ regions, which is consistent with the small rate constants observed for cross relaxation at this temperature. As temperature is increased, however, the thermal population of higher crystal-field levels of $^7F_6$ and $^5D_4$ results in resonant donor and acceptor transitions. Each of these resonances, therefore, involves "hot" transitions on either the donor, the acceptor, or both. Of particular interest is that, above a certain temperature, increasing temperature actually decreases the population of the initial crystal-field levels of many of the resonant crystal-field transitions. This is consistent with the observation of decreasing cross-relaxation rate constants with increasing temperature above some threshold temperature in $CsCdBr_3$ and $CsMgBr_3$.

Figure 8b shows a comparison the calculated line spectra for $^5D_3 \rightarrow {}^7F_0$ emission and $^7F_6 \rightarrow {}^5D_4$ absorption for the three $CsMX_3$ lattices at 160 K. It is clear that different crystal-field transitions are in resonance in each compound. It will be shown later in this section that this difference accounts for the observed difference in the temperature dependence of cross relaxation. We note that the variance in the relative positions of the "centers" of the donor $^5D_3 \rightarrow {}^7F_0$ and acceptor $^7F_6 \rightarrow {}^5D_4$ transition regions relative to each other is only $\sim$30 cm^{-1} across the series.

The curly bracket in $CsMgCl_3$ donor spectrum in Figure 8b. indicates where $^5G_6,^5L_{10} \rightarrow {}^7F_0$ emission from thermally populated $^5G_6,^5L_{10}$ levels is in resonance with $^7F_6 \rightarrow {}^5D_4$ absorption. These transitions are not in resonance in the $CsCdBr_3$ and $CsMgBr_3$ hosts. Unlike $CsCdBr_3$ and $CsMgBr_3$, therefore, the cross relaxation rate constant, k_{cr}, for $CsMgCl_3$ does not show any significant decline with increasing temperature at higher temperatures because the decreasing contribution from $^5D_3 \rightarrow {}^7F_0/{}^7F_6 \rightarrow {}^5D_4$ resonance is at least partially compensated by the increasing contribution from $^5G_6,^5L_{10} \rightarrow {}^7F_0/{}^7F_6 \rightarrow {}^5D_4$ resonance. These additional resonances in $CsMgCl_3$ occur mainly because of the smaller separation between the $^5D_3$ and $^5G_6,^5L_{10}$ multiplets in this lattice relative to $CsCdBr_3$ and $CsMgBr_3$, which is readily apparent when comparing the $^7F_6 \rightarrow {}^5D_3$ excitation spectra shown in Figure 4.

The temperature dependence of the overall effective resonance between donor emission and acceptor absorbance is most easily evaluated by transforming the donor and acceptor line spectra, as shown in Figure 8, into Gaussian spectra and integrating the product of the two. The resulting spectral overlap integrals can be expressed as

$$\text{spectral overlap} = \int_0^\infty \left\{ \sum_{i,j} \left(\frac{N}{N_T}\right)_i \left(\frac{N}{N_T}\right)_j e^{-(\bar{\nu}-\bar{\nu}_i)^2/2\sigma} e^{-(\bar{\nu}-\bar{\nu}_j)^2/2\sigma} \right\} d\bar{\nu} \quad (8)$$

where the sum is over all donor (i) and acceptor (j) transitions; $\bar{\nu}_i$ and $\bar{\nu}_j$ are the donor and acceptor transition energies (in cm^{-1}), respectively; $(N/N_T)_i$ and $(N/N_T)_j$ are the fractional Boltzmann populations of the initial crystal-field levels of the donor and acceptor transitions, respectively; and σ is the standard deviation of the Gaussian distribution. The temperature dependence of the spectral overlap integral is manifested in the $(N/N_T)_i(N/N_T)_j$ term. Note that eq 8 does not take into account differences in the oscillator strengths of the individual crystal-field transitions.

Figure 9 shows the temperature dependence of the donor−acceptor spectral overlap integrals, as calculated using eq 8 ($\sigma = 10$ cm^{-1}), for each of the three lattices. Comparing Figures 7 and 9, one sees that the *relative trends* in the temperature dependence of cross relaxation in the three lattices, in terms of relative sensitivity to temperature and in terms of temperature at which maximum cross relaxation efficiency is achieved, is well explained in terms of the overlap integrals. For example, the overlap integrals predict that cross relaxation in $CsMgBr_3$ will be the most sensitive to temperature and will peak at the lowest temperature of the three hosts. In contrast, the overlap integral for $CsMgCl_3$ peaks at the highest temperature, after which it suffers the least severe decline in overlap with increasing temperature. The correlation between the overlap integrals and the relative temperature dependence of cross relaxation is impressive, considering that our overlap integrals do not take into account differences in oscillator strengths for the individual crystal-field transitions or the temperature dependence of the zero-phonon line widths.

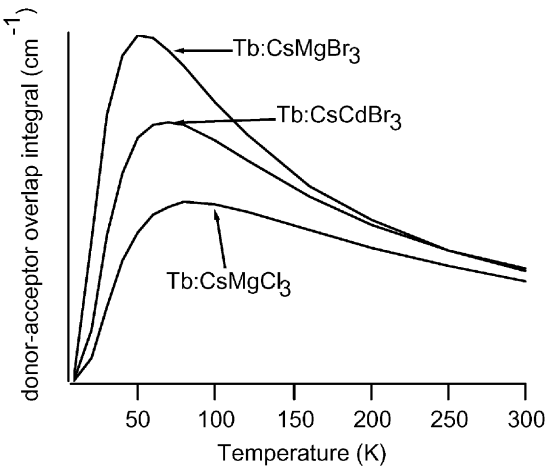

Figure 9. Temperature dependence of the donor−acceptor spectral overlap integrals, as calculated using eq 8 ($\sigma = 10$ cm^{-1}) for each of the three $CsMX_3$ lattices. We note that the overlap integrals will be identical for both the $^5D_3 \rightarrow {}^5D_4/{}^7F_6 \rightarrow {}^7F_0$ and the $^5D_3 \rightarrow {}^7F_0/{}^7F_6 \rightarrow {}^5D_4$ spectral regions.

We note that it can be shown mathematically that the overlap integrals, as defined in eq 8, will be identical for both the $^5D_3 \rightarrow {}^5D_4/{}^7F_6 \rightarrow {}^7F_0$ and the $^5D_3 \rightarrow {}^7F_0/{}^7F_6 \rightarrow {}^5D_4$ spectral regions. This is simply a consequence of the same four multiplets being involved in both of the resonant spectral regions. The preceding overlap analysis is valid, therefore, regardless of the relative contributions of each of the two overlap regions to cross relaxation.

4. Conclusions

This study strongly indicates that $Tb(^5D_3)$ cross relaxation in symmetrical $Tb^{3+}-Tb^{3+}$ pairs in $CsCdBr_3$, $CsMgBr_3$, and $CsMgCl_3$ is due to resonance between zero-phonon crystal-field transitions on the donor and acceptor. Cross relaxation in these systems is, therefore, "resonant", in the sense that only donor and acceptor transitions with significant direct overlap of the zero-phonon spectral lines participate in active transfer mechanisms.

The temperature dependence of cross relaxation is well-explained in terms of the changing thermal populations of the initial crystal-field levels of resonant donor and acceptor transitions. As a result of the stringent resonance requirement, the temperature dependence and maximum efficiency of cross relaxation is very different in the three hosts, despite the fact that the energy-level structures and optical spectra of Tb^{3+} are all quite similar. Although phonon-assisted processes cannot be discounted, they do not appear to have a significant impact on the temperature dependence of cross relaxation and cannot be used to explain the decreasing cross-relaxation rates with increasing temperature that is observed for $CsCdBr_3$ and $CsMgBr_3$ in the high-temperature range of this study. This result is particularly interesting, because it is often not possible in energy transfer studies to discern whether temperature dependencies arise from phonon-assisted processes, from changes in thermal populations of crystal-field levels, or from some combination of the two.

We point out that it is, perhaps, not so obvious that resonance considerations should so easily outweigh the influences of general transition strengths, donor−acceptor separations, and halide identity. Table 5 shows the $Gd^{3+}-Gd^{3+}$ separations in symmetrical pairs for these hosts at 77 K and room temperature as reported by Henling et al.[1] For multipolar mechanisms, cross-relaxation rate constants should be roughly proportional to R^{-S}

TABLE 5: Gd^{3+}-Gd^{3+} Separations in Symmetrical Pairs at 77K and Room Temperature in $CsCdBr_3$, $CsMgBr_3$ and $CsMgCl_3$ According to Ref 1

	temp (K)	$Gd^{3+}-Gd^{3+}$ separation (Å)
$CsCdBr_3$	RT	6.03
	77	5.93
$CsMgBr_3$	RT	5.89
	77	5.82
$CsMgCl_3$	RT	5.47
	77	5.40

($S = 6, 8, 10$), where R is the donor−acceptor separation. At room temperature, multipolar cross relaxation should be ∼1.8 to ∼2.7 times more efficient in $CsMgCl_3$ compared to $CsCdBr_3$, all other aspects of donor−acceptor interactions being equal. Also, as mentioned in section 3.3, the dipole strengths for the two bromide lattices are ∼1.5 times greater than those for the chloride lattice. Finally, mechanisms involving active participation of the halide bridging ion would favor the bromides over the chloride lattice.[59,60]

These results suggest that resonance may be the dominant factor in determining the efficiency of many of the upconversion processes observed from Ln^{3+} pairs in these hosts. In a comparative study of Er^{3+} upconversion in these same three compounds, McPherson et al. noted that upconversion efficiency did not correlate with Er^{3+}-ion separation and speculated that resonance considerations might be to blame.[34] It may, therefore, be possible to significantly influence, or tune, the upconversion properties of lanthanide pairs in these hosts using, for example, magnetic fields.

As mentioned previously, the energy transfer processes discussed in this paper are essentially resonant. It would be interesting to conduct a similar comparative study on donor/acceptor systems for which the energy mismatch between the donor and acceptor transitions was large compared to the zero-phonon line widths of the crystal-field transitions but still smaller than the phonon-cutoff of the lattice. In such systems, it is unclear as to whether spectral overlap considerations could be so closely correlated with energy transfer behavior. Because the phonon cutoff in these crystals is quite low, even the highest-energy phonons have relatively long wavelengths. Holstein and co-workers have shown that single-phonon assisted energy transfer processes can be inefficient when the donor−acceptor separation is equal to, or shorter than, the phonon wavelength.[61] In such cases, two-phonon-assisted energy transfer mechanisms might dominate, and for such mechanisms, there is no direct correlation between transfer efficiency and spectral overlap.

Acknowledgment. This material is based on work supported in part by the U.S. Army Research Laboratory and the U.S. Army Research Office under grant number DAAG55-98-1-0264. Additional funding was provided by NSF-EPSCoR (Award No. 0082978). Acknowledgment is made to the donors of the Petroleum Research Fund, administered by the ACS, for partial support of this research.

References and Notes

(1) Henling, L. M.; McPherson, G. L. *Phys. Rev. B* **1977**, *16*, 4756.
(2) Blasse, G.; Wolfert, A.; McPherson, G. L. *J. Solid State Chem.* **1985**, *57*, 396.
(3) Popova, M. N.; Chukalina, E. P.; Malkin, B. Z.; Iskhakova, A. I.; Antic-Fidancev, E.; Porcher, P.; Chaminade, J. P. *Phys. Rev. B* **2001**, *63*, 075103−1.
(4) Chukalina, E. P.; Popova, M. N.; Antic-Fidancev, E.; Chaminade, J. P. *Phys. Lett. A* **1999**, *258*, 375.
(5) Burdick, G. W.; Richardson, F. S *J. Alloys Compounds* **1998**, *275*−*277*, 379. Burdick, G. W.; Richardson, F. S *Chem. Phys.* **1998**, *228*, 81.
(6) Murdoch, K. M.; Cockroft, N. J. *Phys. Rev. B* **1996**, *54*, 4589.
(7) Antic-Fidancev, E.; Lemaitre-Blaise, M.; Chaminade, J. P.; Porcher, P. *J. Alloys Compounds* **1995**, *225*, 95.
(8) Neukum, J.; Bodenschatz, N.; Heber, J. *Phys. Rev. B* **1994**, *50*, 3536.
(9) Schäfer, U.; Neukum, J.; Bodenschatz, N.; Heber, J. *J. Lumin.* **1994**, *60*/*61*, 633.
(10) Heber, J.; Schäfer, U.; Neukum, J.; Bodenschatz, N. *Acta Phys. Pol., A* **1993**, *84*, 889.
(11) Ramaz, F.; Macfarlane, R. M.; Vial, J. C.; Chaminade, J. P.; Madéore, F. *J. Lumin.* **1993**, *55*, 173.
(12) Chaminade, J. P.; Macfarlane, R. M.; Ramaz, F.; Vial, J. C. *J. Lumin.* **1991**, *48*/*49*, 531.
(13) Virey, E.; Couchaud, M.; Faure, C.; Ferrand, B.; Wyon, C.; Borel, C. *J. Alloys. Compounds* **1998**, *275*−*277*, 311.
(14) Quagliano, J. R.; Cockroft, N. J.; Gunde, K. E.; Richardson, F. S. *J. Phys. Chem.* **1996**, *100*, 9812.
(15) Macfarlane, R. M.; R. M.; Ramaz, F.; Vial, J. C. *J. Lumin.* **1992**, *53*, 244.
(16) Barthou, C.; Barthem, R. B. *J. Lumin.* **1990**, *46*, 9.
(17) Barthem, R. B.; Buisson, R.; Cone, R. L. *J. Chem. Phys.* **1989**, *91*, 627.
(18) Barthem, R. B.; Buisson, R.; Madéore, F.; Vial, J. C.; Chaminade, J. P. *J. Phys. (Paris)* **1987**, *48*, 379.
(19) Barthem, R. B.; Buisson, R.; Vial, J. C.; Chaminade, J. P. *J. Phys., Colloq.* **1985**, *C7*-113.
(20) Pellé, F.; Gardant, N.; Genotelle, M.; Goldner, P.; Porcher, P. *J. Phys. Chem. Solids* **1995**, *56* , 1003.
(21) May, P. S.; Sommer, K. D. *J. Phys. Chem. A* **1997**, *101*, 9571.
(22) Lammers, M. J. J.; Blasse, G. *Chem. Phys. Lett.* **1986**, *126*, 405.
(23) Berdowski, P. A. M.; Lammers, M. J. J.; Blasse, G. *J. Chem. Phys.* **1985**, *83*, 476.
(24) Tigréat, P. Y.; Doualan, J. L.; Moncourgé, R.; Ferrand, B. *J. Lumin.* **2001**, *94*−*95*, 107.
(25) Wermuth, M.; Riedener, T.; Güdel, H. U. *Phys. Rev. B* **1998**, *57*, 4369.
(26) Wermuth, M.; Güdel, H. U. *Chem. Phys. Lett.* **2000**, *323*, 514.
(27) Malkin, B. Z.; Iskhakova, A. I.; Tarasov, V. F.; Shakurov, G. S.; Heber, J.; Altwein, M. *J. Alloys. Compounds* **1998**, *275*−*277*, 209.
(28) Müller, P.; Wermuth, M.; Güdel, H. U.; *Chem. Phys. Lett.* **1998**, *290*, 105.
(29) Mujaji, M.; Jones, G. D.; Syme, R. W. G. *Phys. Rev. B* **1993**, *48*, 710.
(30) Mujaji, M.; Jones, G. D.; Syme, R. W. G. *J. Lumin.* **1992**, *53*, 473.
(31) Pellé, F.; Goldner, P. *Opt. Mater.* **1994**, *4*, 121.
(32) Bordallo, H. N.; Barthem, R. B.; Barthou, C. *Solid State Comm.* **1994**, *92*, 721.
(33) Pellé, F.; Goldner, Ph. *Phys. Rev. B* **1993**, *48*, 9995.
(34) McPherson, G. L.; Gharavi, A.; Meyerson, S. L. *Chem. Phys.* **1992**, *165*, 361.
(35) Cockroft, N. J.; Jones, G. D.; Nguyen, D. C. *Phys. Rev. B* **1992**, *45*, 5187.
(36) McPherson, G. L.; Meyerson, S. L. *Chem. Phys. Lett.* **1990**, *167*, 471.
(37) Cockroft, N. J.; Jones, G. D.; Syme, R. W. G. *J. Lumin.* **1989**, *43*, 275.
(38) Heber, J.; Lange, M.; Altwein, M.; Malkin, B. Z.; Rodionova, M. P. *J. Alloys Compounds* **1998**, *275*−*277*, 181.
(39) Bodenschatz, N.; Neukum, J.; Heber, J. *J. Lumin.* **1996**, *66*/*67*, 213.
(40) Gamelin, D. R.; Luethi, S. R.; Güdel, H. U. *J. Phys. Chem. B* **2000**, *104*, 11045.
(41) Malkin, B. Z.; Leushin, A. M.; Iskhakova, A. I.; Heber, J.; Altwein, M.; Moller, K.; Fazlizhanov, I. I.; Ulanov, V. A. *Phys. Rev. B* **2000**, *62*, 7063.
(42) Hehlen, M. P.; Kuditcher, A.; Rand, S. C.; Luthi, S. R. *Phys. Rev. Lett.* **1999**, *82*, 3050.
(43) Goldner, P.; Pellé, F.; Auzel, F. *J. Lumin.* **1997**, *72*−*74*, 901.
(44) Goldner, P.; Pellé, F.; Meichenin, D.; Auzel, F. *J. Lumin.* **1997**, *71*, 137.
(45) Hehlen, M. P.; Kuditcher, A.; Rand, S. C.; Tischler, M. A. *J. Chem. Phys.* **1997**, *107*, 4886.
(46) Cockroft, N. J.; Murdoch, K. M. *J. Lumin.* **1994**, *60*/*61*, 891.
(47) Goldner, P.; Pellé, F. *J. Lumin.* **1994**, *60*/*61*, 651.
(48) McPherson, A. M.; McPherson, G. L. *Solid State Commun.* **1981**, *37*, 501.
(49) Gharavi, A. R.; McPherson, G. L. *J. Opt. Soc. Am. B* **1994**, *11*, 913.
(50) Xiao, L. S.; Lang, M.; May, P. S. *J. Phys. Chem. A* **2000**, *104*, 209.

(51) Meyer, G.; Morss, L. R., Eds.; *Synthesis of lanthanide and actinide compounds*; Kluwar Acedemic Publishers: Boston, MA, 1991. Meyer, G.; Dotsch, S.; Staffel, T. *J. Less Common Met.* **1987**, *127*, 155.

(52) Both effects are nicely illustrated in each of the following two studies: McLaughlin, R. D.; Conway, J. G. *J. Chem. Phys.* **1963**, *38*, 1037. Baumert, R.; Pelzl, R. B.; Hüfner, *S. Solid State Comm.* **1975**, *16*, 345.

(53) Carnall, W. T.; Goodman, G. L.; Rajnak, K.; Rana, R. S. *J. Chem. Phys.* **1989**, *90*, 3443. Carnall, W. T.; Goodman, G. L.; Rajnak, K.; Rana, R. S. Argonne National Laboratory report ANL-88-8, 1988.

(54) Reisfeld, R.; Jørgensen, C. K. *Inorganic chemistry concepts, vol. 1*: *lasers and excited states of rare earths*; Springer-Verlag: New York, 1977.

(55) Görller-Walrand, C.; Binnemans, K. *Handbook on the physics and chemistry of rare earths*; Elsevier: New York, 1998; Vol. 25, Chapter 167.

(56) Gruen, D. M.; DeKock, C. W.; McBeth, R. L. *Adv. Chem. Ser.* **1967**, *71*, 102.

(57) Blasse, G. *Struct. Bond.* **1976**, *26*, 43.

(58) Mehta, V.; Guillot-Noël, O.; Simons, D.; Gourier, D.; Goldner, P.; Pellé, F. *J. Alloys Compounds* **2001**, *323*−*324*, 308.

(59) Mironov, V. S.; Kaminskii, A. A. *Phys. Stat. Sol.* (*B*) **1994**, *183*, 481.

(60) Scholes, G. D.; Ghiggino, K. P.; Oliver, A. M.; Paddon-Row, M. N. *J. Phys. Chem.* **1993**, *97*, 11871 and references therein.

(61) Holstein, T.; Lyo, S. K.; Orbach, R. *Top. Appl. Phys.* **1981**, *49* (Laser Spectrosc. Solids), 39.